Nanoelectronic Modeling (NEMO): A New Quantum Device Simulator

Dan Blanks, Gerhard Klimeck, Roger Lake, *R. Chris Bowen, **William R. Frensley, **Manhua Leng, and *Chenjing L. Fernando

Raytheon TI Systems, Dallas, TX 75265
*Texas Instruments Inc., Dallas, TX 75265
**School of Engineering, The University of Texas at Dallas, Richardson, TX 75083

Abstract

Device simulation is a standard practice in the design of state-of-the-art semiconductor devices. These simulations are based on semi-classical models that break down as device geometries approach atomic dimensions. Conventional device simulators may include effects such as tunneling and quantum confinement in an ad hoc *manner, but such approaches are applicable only over a narrow range of device designs and operating conditions. To address this problem, we developed NEMO (NanoElectronic MOdeling), a new quantum device design tool that simulates a wide variety of quantum devices including RTDs, HEMTs, HBTs, superlattices, and Esaki diodes. NEMO uses a non-equilibrium Green's function formalism to treat the effects of quantum charging, bandstructure, and incoherent scattering. A collection of models allows the user to trade off simulation accuracy with speed and memory requirements. This approach addresses the diverse needs of the engineer who desires a black-box design tool and the theorist who is interested in a detailed investigation of the physics. Here we present an overview of the theoretical methodology, graphical user interface features, and simulations for various devices.*

1. Introduction

NASA and the semiconductor industry have a long history of mutually beneficial interaction. The race for the Moon in the 1960's spurred the need for on-board electronics with reduced weight and greater functionality. Prior to the development of the commercial IC market, the space program along with the military provided major incentives for government funding of semiconductor devices far beyond the immediate needs of the marketplace. Consequently, the eventual triumph of the Apollo mission was also a victory for the semiconductor industry and played a significant factor in today's dominance of US industry in the world commercial semiconductor market.

Just as microelectronics was the key to the early days of space exploration, nanoelectronics will be essential for its future. Declining budgets have only increased the need for smaller and better electronics. In addition to the obvious benefits of reduced weight and size, nanoelectronic devices possess functionality not available in conventional devices. For example, resonant tunneling devices (RTD) exhibit negative differential resistance (NDR) with the possibility of Terahertz switching speeds. Since they are majority-carrier devices, RTD's can operate from cryogenic temperatures to room temperature. The combination of smaller size and majority-carrier operation also enhances resistance to radiation, a key problem in space-based systems. Even more advanced structures such as quantum dots and single-electron transistors (SET) hold the potential for extremely dense three-dimensional arrays of nanoelectronic devices.

Despite these exciting possibilities, nanoelectronic devices are still in their relative infancy. The expense and difficulty of device fabrication precludes simply building and testing vast arrays of quantum devices. To focus efficiently on the best design, engineers need a tool that predicts electronic characteristics as a function of the device geometry and composition. In a more scientific mode, such a simulator would greatly enhance the understanding of quantum effects that drive the transport process and provide a means to investigate new device concepts.

Even conventional semiconductor devices require a correction for quantum effects associated with the smaller device features. MOS devices, for example, exhibit electron confinement effects in the inversion layer. This phenomena is a function of decreasing oxide thickness rather than the overall size of the device. Quantum effects becomes important as the oxide layer thickness decreases below the 30 Å, which will soon be a

standard for manufactured integrated circuits. Problems of this nature will become more prevalent as device geometries continue to shrink.

Nanoelectronic device modeling requires a fundamental quantum-mechanical approach. State-of-the-art semiconductor device simulators based on drift-diffusion equations (e.g. PISCES) or Boltzmann's equation (e.g., DAMOCLES [1]) can only include these effects in an *ad hoc* manner. Therefore, the semiconductor industry needs a new fully quantum-mechanically based TCAD tool.

To address this problem, we developed a general purpose 1-D quantum device simulator called NEMO (NanoElectronic MOdeling). NEMO can simulate a wide variety of nanoelectronic devices, including RTD, HEMTs, Esaki diodes, and three terminal devices like the bipolar quantum tunneling transistor. NEMO encompasses the diverse needs of the engineer who wants a black-box design tool and the theorist interested in a detailed investigation of the physics. It has a collection of models that allows the user to trade off between calculation speed and accuracy. NEMO also includes a graphical user interface (GUI) that enables parameter entry, calculation control, display of calculation results, and *in-situ* data analysis methods.

This paper reviews the capabilities of NEMO, summarize the theoretical approach, and give examples of several NEMO simulations.

2. NEMO Theory

2.1 Overview

A full discussion of the NEMO theory is beyond the scope of this article. Here we highlight the theoretical framework and the available transport models. A comprehensive description of the NEMO theory is in reference [2] with a recent amendment in reference [3]. For a list of references to work on resonant tunneling diodes we refer the reader to the list provided in reference [2]. The first examples of our generalized boundary conditions that allow us to treat realistically long devices are in reference [4]. Examples of RTD simulations including effects due to scattering and bandstructure [5-9] are also in the literature. Numerical tools developed for this project are discussed in references [9, 10]. Boykin [11-13] provided the sp3s* full band parameters for typical III-V materials and developed numerical tools that allow for the numerical treatment of full bandstructure effects.

Prior to NEMO, most quantum device simulations solved the single particle effective mass Schrödinger equation coupled with Poisson's equation. To make the problem tractable, these simulations employed one or more stringent approximations, including low temperature, low bias, simplified bandstructure, or no scattering. The calculated results were usually limited to a specific type of device operating over a small range of conditions. The transition from research to production requires a more comprehensive TCAD tool that simulates a variety of devices under a wide range of conditions, particularly for room temperature and high voltage operation.

Although the Schrödinger equation approach is widely used, it cannot properly treat incoherent scattering or the electron reservoirs in the contacts. These limitations arise because Schrödinger's equation only models the states of the system for a single electron (dynamics) and not the carrier transport (kinetics). Modifications of the states due to interactions with other particles (electrons, phonons, etc.) must be patched in as effective potentials while another independent equation treats state occupation and carrier transport. This method de-couples the carrier dynamics from the carrier kinetics. In reality, scattering events redistribute the occupation of quantum states, break their coherence, and shift their resonant energies. In addition, the Pauli exclusion principle forbids the scattering into occupied states. All of these phenomena couple the dynamic and kinetic processes. Moreover, the Schrödinger equation-based models assume flat band profiles for the electron reservoirs whereas realistic devices exhibit complex band bending due to carrier accumulation at the interface.

The non-equilibrium Green function formalism (NEGF) provides a comprehensive framework that couples dynamics and kinetics in a Hamiltonian-based system. It also can apply different approximations in different areas of the device. To use this capability, NEMO divides the device into non-equilibrium and reservoir regions. The non-equilibrium region encloses the quantum well and barrier structures. The remaining reservoir regions encompasses the device contacts and the adjacent layers which act as current sources and sinks. The reservoirs typically have a high electron density and are adequately modeled with a semi-classical relaxation time approximation coupling quantum mechanical states. In the non-equilibrium region, NEMO uses the complete quantum theory to explicitly treat the scattering processes. By concentrating the full quantum calculation on the non-equilibrium region and using a relaxation time approximation elsewhere, NEMO can simulate realistically long structures with spatially non-uniform electron reservoirs.

The essential breakthrough in modeling RTDs is the proper treatment of the reservoirs (relaxation time approximation scattering) and the proper band structure.

For example, we find that NEMO simulations that neglect scattering in the non-equilibrium region are in excellent agreement with experimental measurements for a large set of devices [7], including current vs. voltage (I-V) data of RTDs at room temperature and tunnel current through Si/SiO2/Metal [14] structures. Usually, under high-temperature/high-current conditions, most of the current flows coherently through the resonant states rather than via incoherent processes. Only RTDs operated at low temperature or with low current density require explicit treatment of scattering in the non-equilibrium region.

Because of the complexity and relatively undeveloped nature of the theory, the current NEMO simulator only applies to 1-dimensional devices. We have prototyped a 2-D simulation tool based on NEGF which can be used to analyze ultra-scaled FETs.

The main simulation options can be distinguished by the choice of potential, bandstructure and scattering models. The following sections summarize these options.

2.2 Potential and Charge Models

The two major potential models available in NEMO are Thomas-Fermi and Hartree self-consistent charge calculation. The Thomas-Fermi model uses a semi-classical approximation to calculate charge in the reservoir regions. Charge in the non-equilibrium region is either set to zero or calculated from a quasi Fermi-level linearly interpolated between the contact Fermi levels. The final step uses Poisson's equation to calculate the electrostatic potential and semi-classical charge self-consistently throughout the device.

At best, the Thomas-Fermi model can only give an approximate estimate of charge in the non-equilibrium region and the reservoirs containing quantized states. This is inadequate for devices with appreciable charge build-up in these regions. The Hartree model is more rigorous in that it calculates quantum charging effects self-consistently in the non-equilibrium region as well as the terminals. The LDA approximation [15] takes exchange and correlation effects into account. While the Hartree calculation may be computed over the entire device, we usually only apply it to the region of the device that contains quantum states and use the semi-classical approximation elsewhere. Limiting the calculation range in the manner can dramatically reduce computation time with little effect on the calculation accuracy.

The Hartree model is usually more accurate than the Thomas-Fermi approach, particularly in the quantum well region where charge buildup can have a dramatic influence on device behavior. Alternatively, the Thomas-Fermi calculation is much faster and yields a potential profile very close to the Hartree model. In fact, the Thomas-Fermi calculation is so fast that it can generate band profile curves as we change the applied bias in real-time. The Resonances mode of the NEMO GUI uses this capability.

Another potential model available in NEMO is the linear potential drop in the non-equilibrium region. This models assumes that the free charge is identical to the doping in the terminals such that the potential is flat in each terminal and drops linearly in the non-equilibrium region.

2.3 Band Structure Models

Detailed understanding of the band structure is even more critical for quantum devices than for most conventional semiconductor devices. Charge can conduct through resonant states at very high energies compared to the band edge of the well material. Simultaneously, the same carriers can tunnel through the band gap of the barrier material where there is an effective imaginary band structure. In both cases, the carriers sample portions of the band structure rarely accessed by semi-classical devices. Even if conduction takes place primarily in a single band, a multiple-band calculation may be required to obtain the proper shape of that band, especially for energies high above the band edge. Thus, NEMO provides a large array of band structure models, including:

- Single band effective mass
- Multiple de-coupled single bands (no transport between the bands, but electrostatic coupling via Poisson's Equation).
- Parameterized single-band which includes band-non-parabolicity derived from several sources of bandstructure data (sp3s*, k•p, tables)
- k•p nearest neighbor 2-bands
- sp^3s^* nearest neighbor 10-bands with and without spin orbit coupling and with and without explicit spin basis.

The appropriate model depends on the details of the device structure and the operating conditions. NEMO allows the user to select among these models to trade off accuracy with speed and memory usage.

An internal database provides all relevant band structure parameters for any standard III-V compound. The user can insert customized parameter values for any material system. The Band Structure dialog discussed in Sec.4.3 provides a user-friendly method to examine these models.

2.4 Scattering Processes

Scattering processes often dominate conduction at higher voltages, particularly in RTDs where scattering is the ultimate limit of the valley current. For the single band models NEMO includes models for the following scattering mechanisms:

- Acoustic phonon
- Polar optical phonon
- Interface roughness
- Alloy disorder

3. NEMO GUI

3.1 Overview

Another important goal of the NEMO project was to make a user-friendly simulator that provides as much control as possible over every aspect of the simulation. Flexibility and ease-of-use are difficult to achieve simultaneously, but given the complexity of quantum device simulations it became clear that both criteria were vital to the program success. Consequently, graphical user interface (GUI) development was a major part of the NEMO program. Here we present an overview of the most important GUI features, including:

- Main Screen
- Device Structure Dialog
- Material Parameters Dialog
- Simulation Parameters Dialog
- Simulation Library Dialog
- Band Structure Dialog
- Plot Features

3.2 Main Screen

The Main Screen shown in Fig. 1 is the central location where the user controls the NEMO simulation. From the Main Screen, you can:

- Raise all of the major NEMO windows.
- Switch between Current vs. Voltage and Resonances mode.
- Enter test conditions (bias, temperature, etc.).
- Initiate and abort a calculation.
- Interrupt a calculation and decide whether to abort or continue.
- Open and save NEMO parameter files
- Open and save files with NEMO calculation results.

The Resonances calculation mode is shown in Fig. 2. Energy resonances refer to the quasi-bound states that form in a quantum well structure. The location of these states in energy and position is critical to the operation of a quantum device since most of the device current flows through these states.

When in the Resonances calculation mode, NEMO displays a calculated band profile with horizontal cursors located at the Fermi levels in each device contacts. The user can directly enter the bias into the Test Conditions box or use the mouse pointer to select the emitter Fermi level cursor. A Thomas-Fermi approximation calculates the band profile so quickly that the band profile follows the Fermi level as the user moves the cursor.

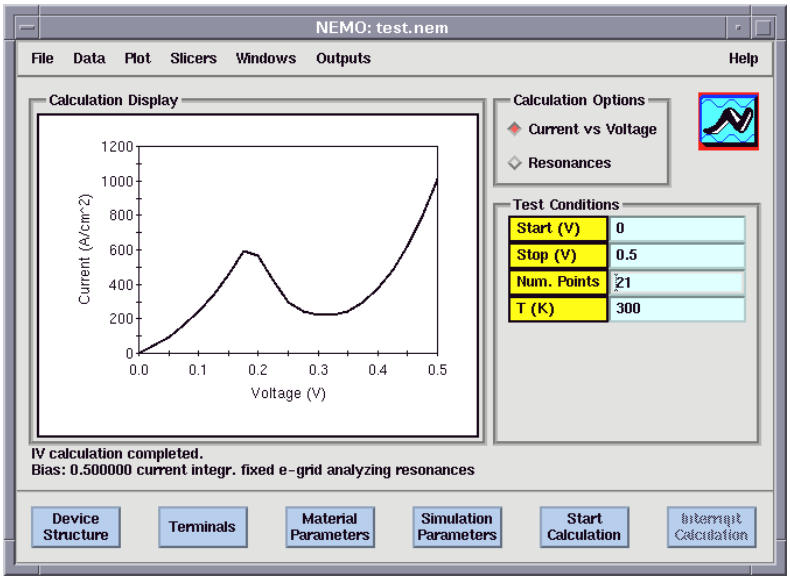

FIG. 1. The NEMO Main Screen set to the Current vs. Voltage mode. The Test Condition panel contains entry boxes for the voltage limits and number of points. When the user presses Start Calculation, NEMO plots the calculated current in the Calculation Display graph. This figure shows the current simulation for a 2-barrier RTD device.

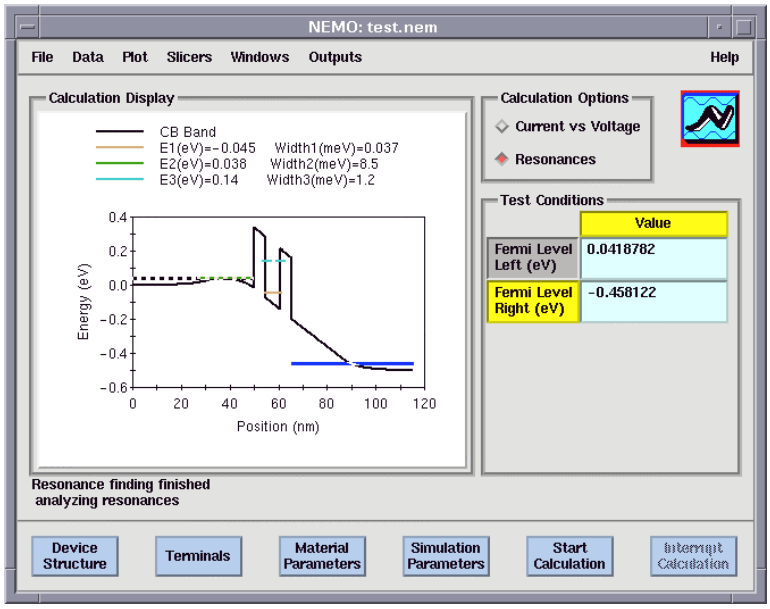

FIG. 2. The NEMO Main Screen in the Resonances mode. The Calculation Display shows the calculated band profile of a 2-barrier RTD under bias with associated energy resonances in the emitter and quantum wells. The Test Condition table contains entry boxes for the emitter (left) and collector (right) quasi-Fermi levels. The emitter level is set either via direct entry into the text box or by selection of the right Fermi level cursor with the mouse pointer. NEMO calculates the band profile in real-time as the user moves the Fermi level. Pressing Start Calculation initiates the energy resonance simulation.

3.3 Device structure dialog

The Device Structure window in Fig. 3 contains a Layer Arrangement spreadsheet for entry of the device layer information. Each row represents one layer in the device and defines layer properties such as composition and thickness.

The Materials list displays compounds that are consistent with the Substrate selection in the Material Options panel. Double-clicking the mouse pointer on an item in the Materials list creates a corresponding entry in the Layer Arrangement table. In this manner, the user can quickly enter very complicated layer arrangements with a minimum of typing. Figure 3 shows the Device Structure dialog for a 2-barrier RTD device.

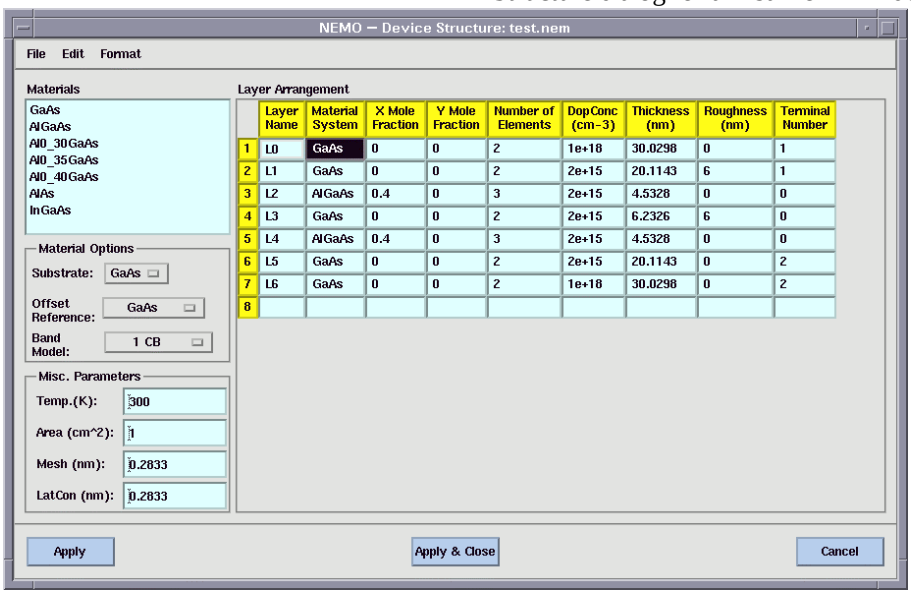

FIG. 3. Device structure dialog box. The layer composition can be entered in a table format from a selection of available materials. General parameters such as temperature, device area and lattice spacing can also be altered.

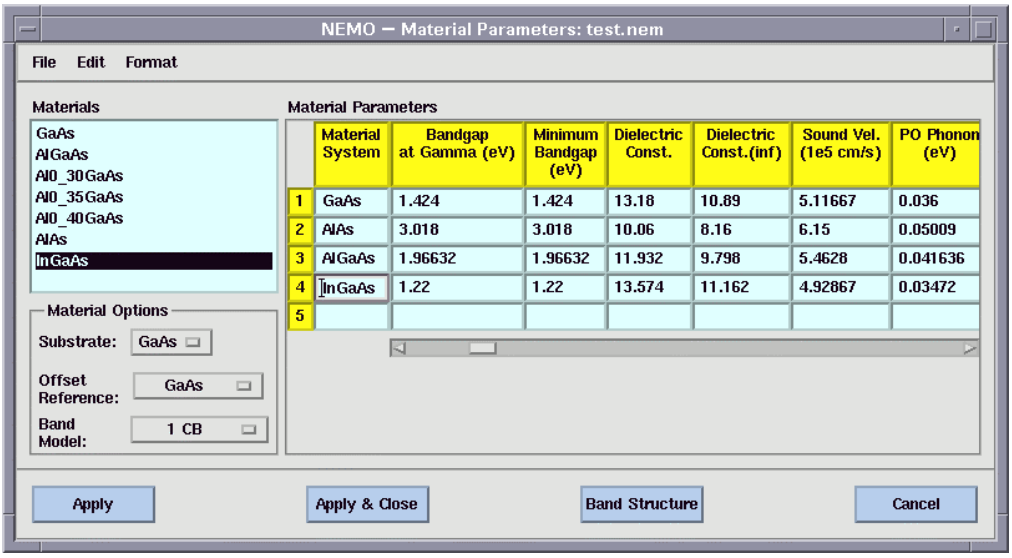

FIG. 4. The NEMO Material Parameters dialog. The Material Parameters table displays relevant material parameter values and allow the user to enter customized values. The user can also create "new" materials with specified material parameters.

3.4 Material parameters dialog

Material parameters include any intrinsic properties relevant to the electronic properties of the compound. Examples include the energy gap, effective mass, and dielectric constant. The proper choice of material parameters is essential to accurate quantum device calculations, particularly for quantum devices where tunneling processes are extremely sensitive functions of material parameter values. NEMO furnishes default parameters for a wide variety of materials and displays them in the Material Parameters dialog in Fig. 4. If the default parameters suffice for the devices of interest, the user never needs bring up the Material Parameters window. However if the user wants to provide customized parameters to the simulation NEMO allows the user to enter his own parameter values for any material. You can even enter a user-defined material with your own customized parameter values.

4. Simulation parameters

4.1 Overview

Simulation parameters control the selection of theoretical models used in the NEMO calculation. NEMO includes different models to calculate the current, potential, charge, scattering processes, and the band structure. The simulation parameters also specify the desired calculation outputs options. To simplify the parameter input process, NEMO uses a hierarchical approach for the display and entry of simulation parameter values. In addition to traditional entry methods (e.g., text boxes, option lists, etc.) NEMO also provides graphical methods to enter regional parameters that depend on relative positions of the device barriers and wells. The next few sections discuss these features.

4.1.1 Simulation parameters -- hierarchical methodology

NEMO has a rich variety of simulation models. While this provides the maximum flexibility in terms of applicability to different types of devices and test conditions, the downside is that NEMO requires over 100 simulation parameters. Traditional device simulators force the users to familiarize themselves with all available simulation parameters and ensure that they are set correctly.

To minimize this burden for the users, NEMO employs an innovative hierarchical approach to input simulation parameters. The top level of this hierarchy specifies the highest level calculation option (Current or Resonances). Subsequent levels contain more detailed options such as the choice of potential model and scattering processes.

For parameter entry, NEMO creates text boxes, radio boxes, and option lists that correspond to the simulation parameters for a single hierarchy level and display them in the Simulation Parameter table as shown in Fig. 5. Each time the user presses Next, NEMO goes through the following process:

- Accept parameter settings for the latest displayed hierarchy level.
- Determine the parameters needed for the next level.
- Create new GUI elements.

- Display new level.

NEMO only displays parameters required by the prior selections. For example, different potential models require different parameter sets. Once the user selects a potential model, NEMO only shows parameters that are consistent with that model. Parameters unique to other models are either not created or are disabled from input.

This method of limiting the displayed parameter set greatly diminishes the burden on the user. For most simulations, the user need only specify high level options in the hierarchy. NEMO provides default settings that usually suffice for the lower-level parameter values. In practice, the user can set the higher level options of interest and then select the Finish button to accept the remaining default parameter settings. NEMO arranges the simulation parameter levels in a scrollable table such that the user can examine the parameter values. The Prev button moves backwards to the previous simulation level. The Start button restarts the input procedure at the top level.

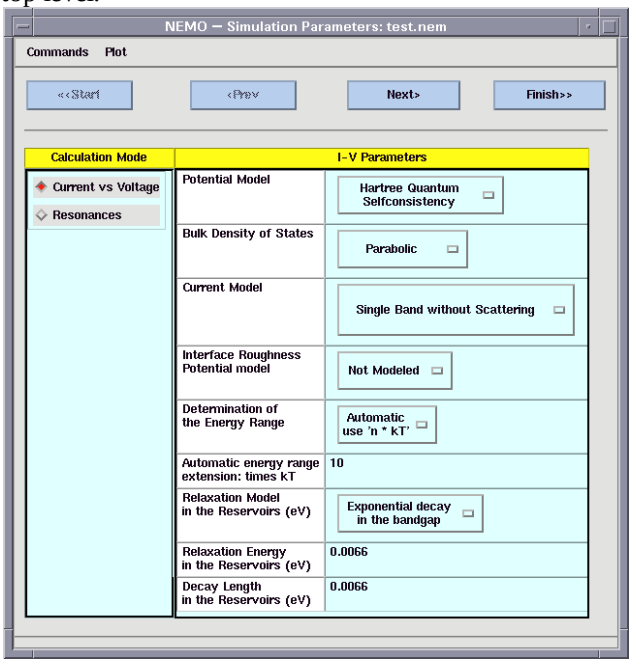

FIG. 5. The NEMO Simulation Parameters dialog. The Simulation Parameters table displays text boxes and option lists for parameter entry.

4.1.2 Simulation parameters -- Output Options

While current vs. voltage is the most commonly viewed output, NEMO can calculate a large range of device characteristics. The Output Options panel shown in Fig. 7 displays selection toggle buttons to select any combination of outputs. If an output requires more

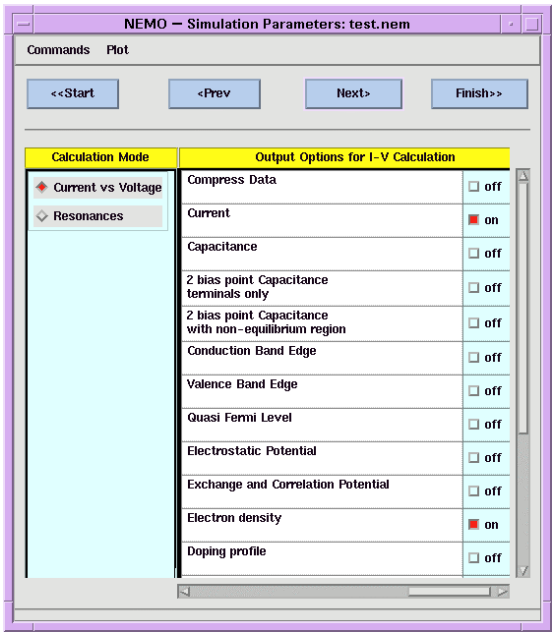

FIG. 6. The NEMO Simulation Parameters dialog set for entry of output options. The user can select any combination of outputs. NEMO automatically creates a plot window for each selected option set.

specific information that needed for the original calculation, NEMO will create the corresponding hierarchical level and display it in a subsequent panel.

4.1.3 Simulation parameters -- graphical parameter entry

One of the key advantages of the NEGF formalism is that it can apply different theoretical algorithms in different regions of the device. To reduce the memory and calculation time, we usually limit the full Green's function calculation to the region surrounding the quantum wells and barriers and use the standard semi-classical approximations elsewhere. The same approach is used to limit the calculations of energy resonances and quantum charge to the areas of interest. These regions are not necessarily coincident, but some regions must be contained within other regions.

To set the proper location for these regions, NEMO displays the band profile with pairs of movable cursors to indicate the boundary locations (Fig. 6). The Fermi level is a movable cursor just as it is in the Main Screen when set to Resonances mode. The real-time band profile calculation provides visual feedback of the behavior of the bands with bias. This capability is essential to estimate the best locations of the region boundaries.

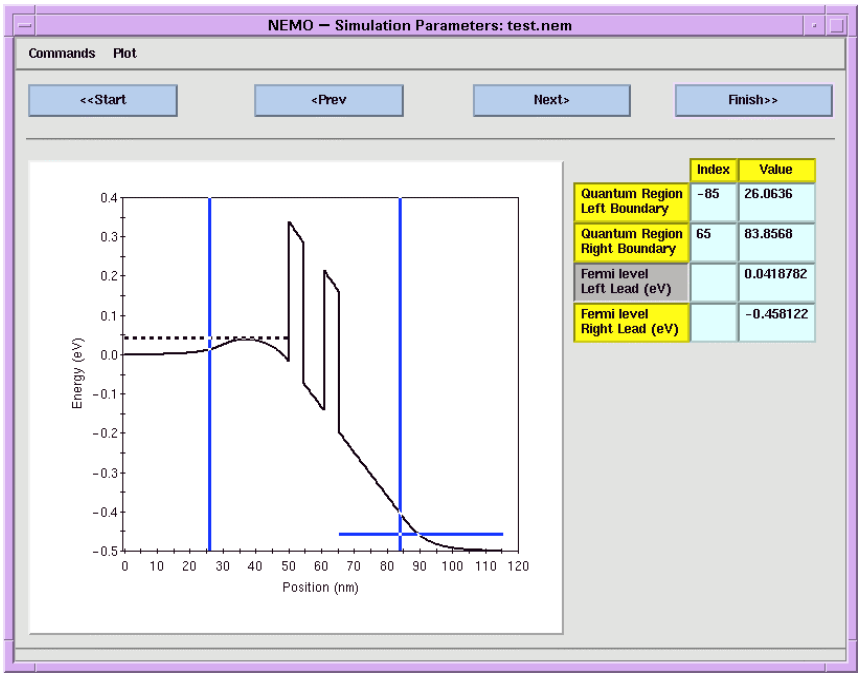

FIG. 7. The NEMO Simulation Parameters dialog set for entry of simulation region boundaries. The user can move the cursors with the mouse pointer or enter values in the corresponding entry box. The horizontal cursor controls the quasi-Fermi level in the emitter contact. The vertical cursors control the left and right region boundaries.

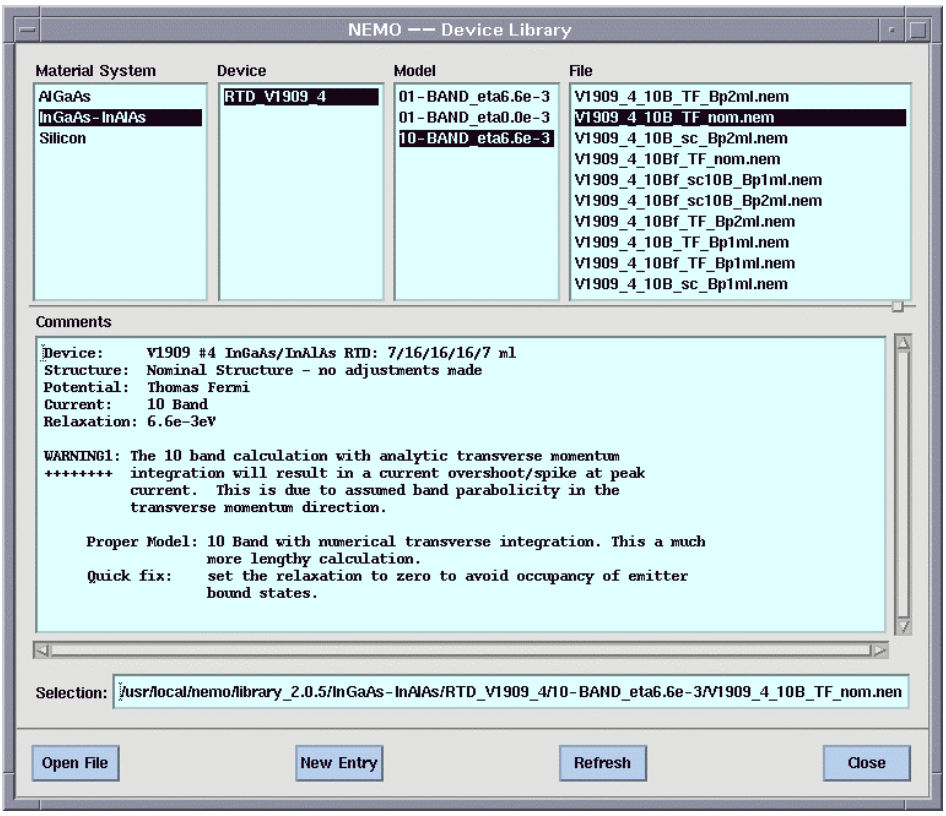

FIG. 8. The NEMO Simulation Library. Selection of an item in the each higher-level category displays associated items in the next category. The Files list displays a list of simulation files with various approaches for performing the calculation. The Comments section gives detailed information about the simulation.

4.2 Simulation library

The Simulation Library is a collection of simulations for a variety of devices. The Simulation Library window (Fig. 8) displays a hierarchy of material systems, devices, and models. The Comments text box explains the application for the simulation selected in the Files list. Users are requested to enter comments into every input file. The comments can be browsed by the library dialog box and can be used to describe more carefully the intended simulation. The library simulations provide an excellent starting point for NEMO calculations. It is usually easier to load one of the library examples and alter the device structure than to create a device and input simulation parameters from scratch.

4.3 Band structure dialog

As discussed earlier in this paper, NEMO includes a collection of band structure models. To examine these models in detail, the Band Structure dialog displays plots of band structure parameters in several forms, including the energy bands, effective mass, and electron density as a function of Fermi level. The example in Fig. 9 illustrates the conduction, heavy-hole, light-hole and split-off bands for GaAs in the <100> (positive k) and <111> (negative k) direction derived from an sp^3s^* model including spin-orbit interaction.

4.4 Plot Features

4.4.1 Plot Slicers

Most of the NEMO calculations generate a 2-D set of data for a given bias point. This data is typically either plotted against position in the device (e.g., band profile) or versus energy (e.g., transmission coefficients). During a current vs. voltage scan, NEMO stores the data for any given output into graphical tool called a Plot Slicer. The Plot Slicer retains the calculation for each bias point. After the scan finishes, the user can move the horizontal slide bar to view the calculation results for any bias point. In effect, the Plot Slicer displays cross-sections of a 3-dimensional data set. Calculated outputs that vary with position can also be switched to show cross-sections in

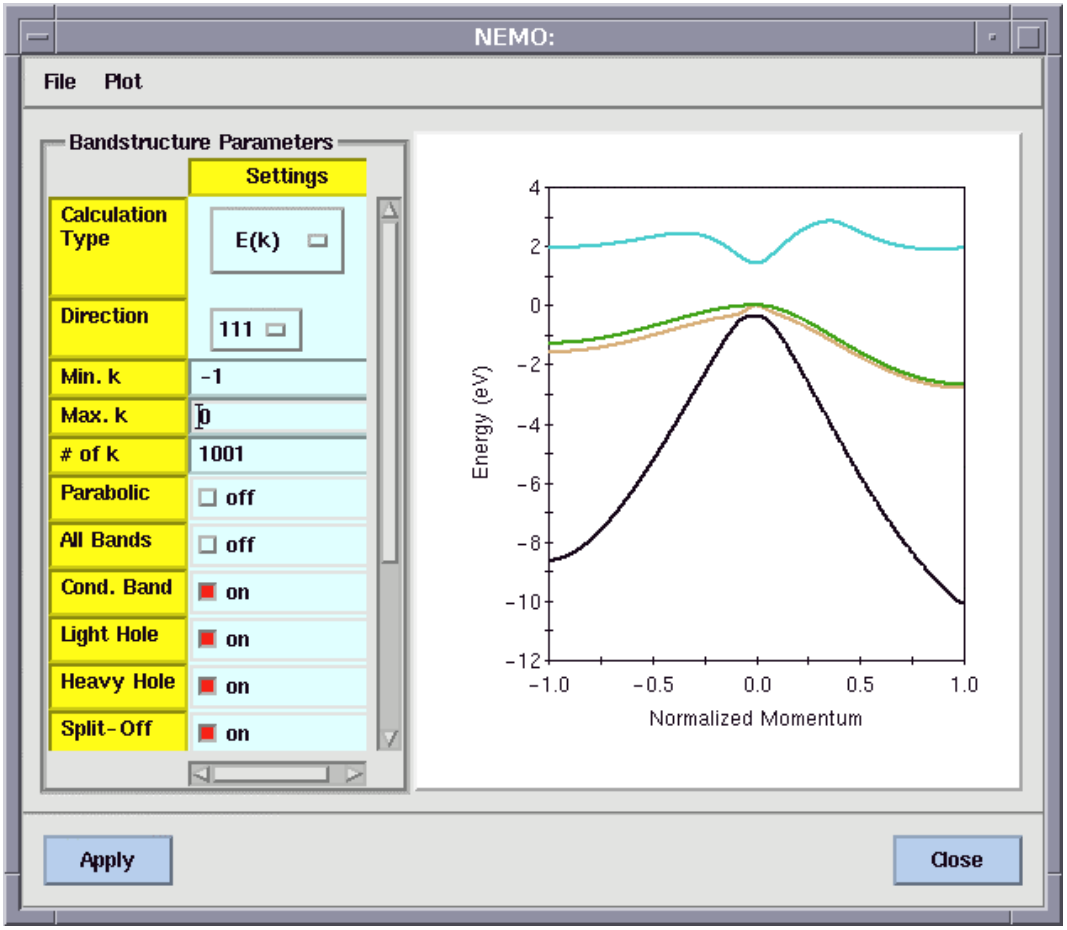

FIG. 9. NEMO's Band Structure Dialog. The conduction, heavy-hole, light-hole and split-off band is plotted for GaAs in the <100> (positive k) and <111> (negative k) direction. This dispersion is derived from an sp3s* parameter set including spin-orbit interaction.

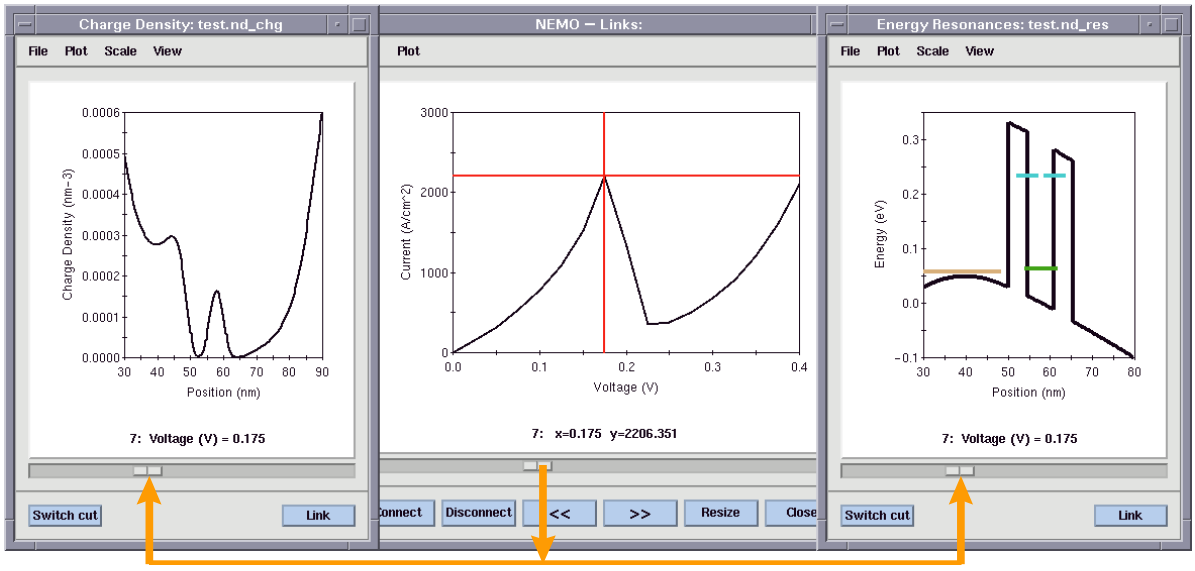

FIG. 10. Plot Slicer coupling multiple output windows. The simulation output can be explored interactively.

which the slide bar moves between different positions and the data is plotted vs. the applied bias.

The Plot Linker connects all of the active Plot Slicers to a single slide bar. A cross-hairs cursor displays the corresponding position in the current vs. voltage scan. As the main slide bar moves, all of the other Plot Slicers move in unison to the same bias. The buttons marked with "<<" and ">>" position the slide bar to voltages at local minima and maxima of the current calculation. The Plot Linker is extremely useful for analyzing device characteristics. Figure 10 shows examples of Plot Slicers for charge and energy resonances of a 2-barrier RTD linked to the I-V calculation.

4.4.2 3-D plots

Multiple 2-D PLOTS can be assembled into a 3-D plot. The 3-D plot tool displays a surface plot of most of the NEMO data sets. The user has control over many display attributes such as colors, grid density, number of contours, etc. Figure 11(a) shows the band profile as a

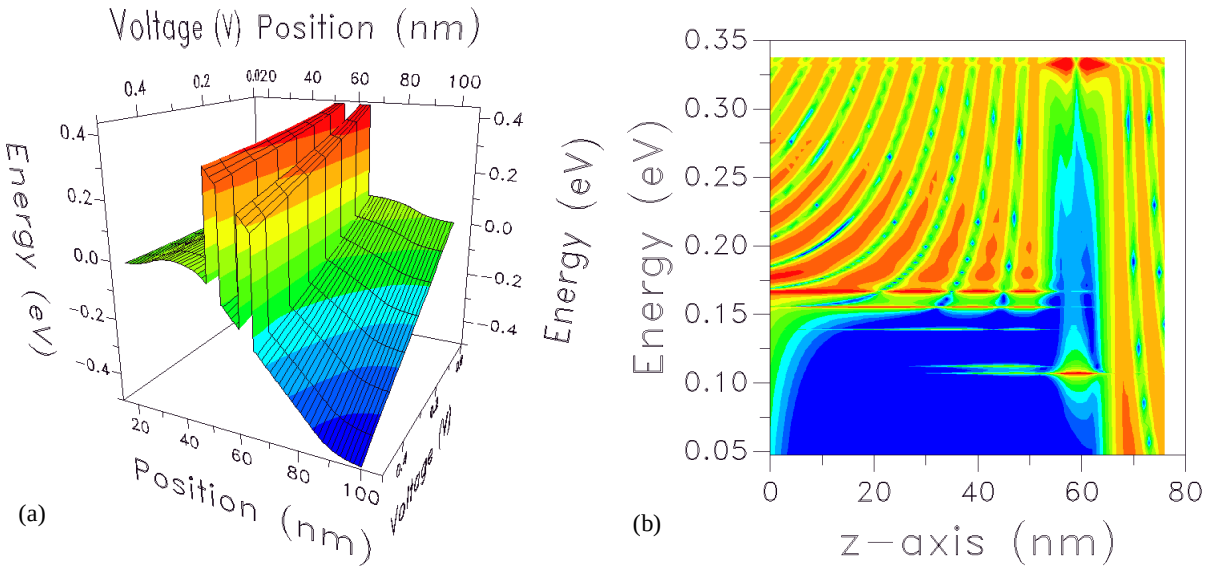

FIG. 11. (a) 3-D visualization of the conduction band edge as a function of position and applied bias. Slices through either the position or the voltage axis can be taken to analyze the band edge in more detail. (b) 3-D contour plot visualization of the density of states of an RTD. The central ground state in the RTD is visible at about 60 nm and 0.10 eV. The first excited state is visible at about 0.34 eV. On the emitter side of the RTD a two emitter quasi-bound states are visible. The ground state in the triangular emitter well is strongly coupled to the central resonance.

function of position and voltage.

4.4.3 Contour plots

The 3-D plot tool can also display contour plots of the same 3-D surface data. Most of the same format controls for the 3-D tool apply to the contour plot.

This sample plot in Fig. 11(b) shows the density of states for a 2-barrier RTD device as a function of energy and position.

5. NEMO Simulations

The RTD device was chosen as an ideal "straw man" for the comparison of calculation to experiment. An RTD utilizes quantum resonant states as the basis of its operation, is relatively simple to construct, has as a reasonably 1-dimensional geometry, and can operate at room temperature. However, we also stressed that NEMO had to operate on any general 1-dimensional device. In the course of the NEMO program, we have simulated HEMT, MOS, and Esaki diodes.

As examples we consider in the following sections high performance room-temperature InP based RTDs, examine a scattering limited RTD in the GaAs/AlAs material system and look at several MOS device simulations.

5.1 High Performance Room Temperature InP-based RTDs

State-of-the-art InP-based RTDs are being developed for circuit applications such as low power memory cells [16], high speed adders [17] and high speed logic [18]. Depending on the application RTDs must be designed to provide either a low [16] or a high [17] current density. Quantitative modeling of such devices is expected to reduce the device development cycle time significantly [19].

We demonstrate NEMO's ability to quantitatively model pseudomorphic InP-based RTDs which can include lattice matched $In_{0.53}Ga_{0.47}As$, $In_{0.52}Al_{0.48}As$, and pseudomorphic AlAs. We present quantitative simulations of strained and unstrained InP-based RTDs that include quantum charge self-consistency (Hartree) in a full band (sp^3s^*) model. The quantitative modeling of these devices requires accurate modeling of the bandstructure for each material. The strained AlAs barriers and InAs wells have altered bandgaps, band-offsets, effective masses and relative line-ups of Γ and X valley from their respective bulk values. Important bandstructure features to be modeled are the non-parabolicity of the $In_{0.53}Ga_{0.47}As$ and InAs and the complex band wrapping in the $In_{0.52}Al_{0.48}As$ and AlAs barriers. All these features combined required us to develop sp^3s^* bandstructure parameters optimized for the conduction and valence bands including spin-orbit interactions [13]. Not only is accurate bandstructure necessary, but a self-consistent calculation of the

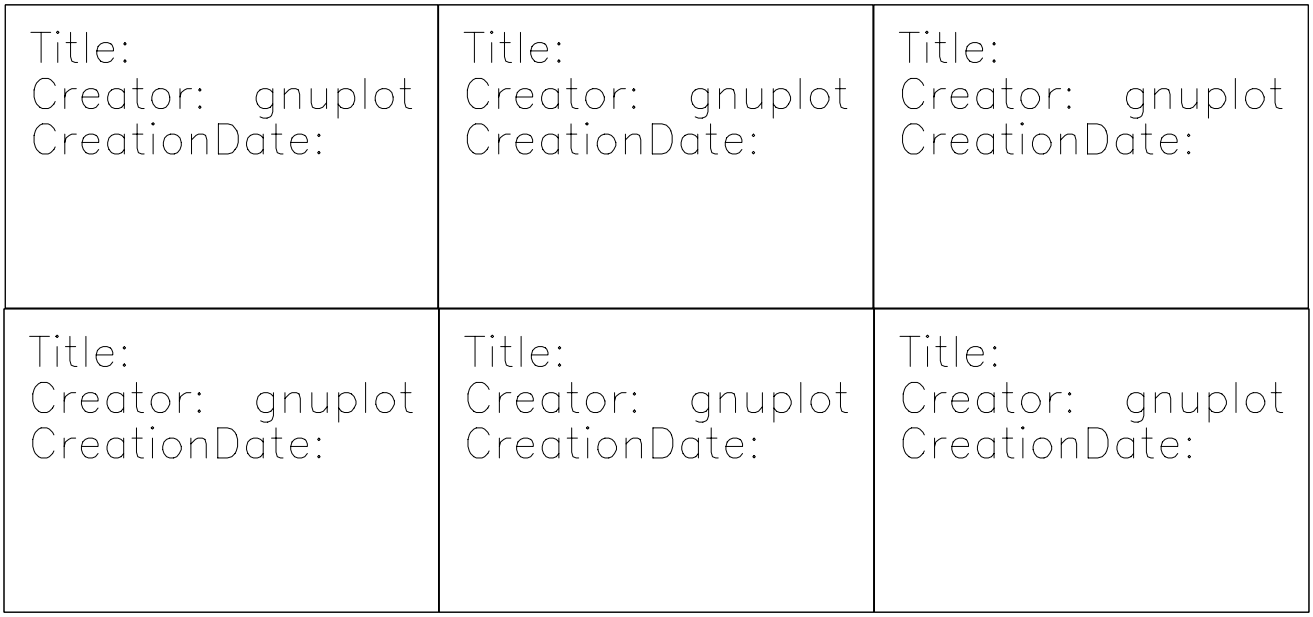

FIG. 12. Test matrix of an unstrained $In_{0.53}Ga_{0.47}As/In_{0.52}Al_{0.48}As$ RTD system on an InP substrate. The symmetric device V1909 #2 has a nominal well and barrier thickness of 30Å/10 mono-layer (ml) and 47Å/16ml, respectively. The devices are symmetrically clad with 20Å/7ml undoped, 500Å low doping ($2x10^{18}$ cm^{-3}) and 500Å high doping ($5x10^{18}$ cm^{-3}) spacer/contact layers. (a-c) Variation of the well thickness ((a) 11ml, (b) 12 ml, (c) 16 ml). (c-f) Variation of the undoped spacer layer ((c) 7 ml, (d) 20 ml, (e) 40 ml, (f) 68 ml).

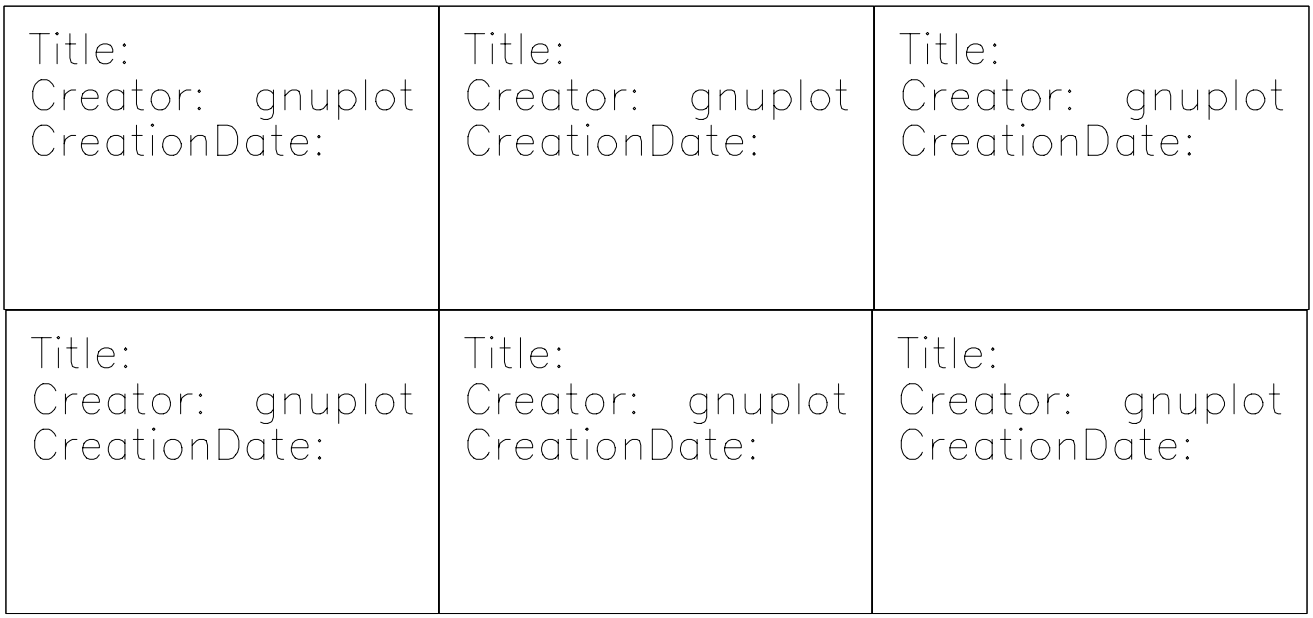

FIG. 13. Test matrix of a strained InGaAs/AlAs RTD system. One of the AlAs barriers is increased in thickness by one monolayer at a time. The cladding is the same as described in FIG. 12. (a-c) Comparison of experimental and simulated I-V's. Forward bias (thicker collector barrier) shows a higher peak current at a higher voltage. (d-f) Potential profiles calculated for device #3 in forward and reverse bias for applied voltages of 0.28 V and 0.52 V. For comparison we spatially reverse the order of the layers for the reverse bias direction. (d) 0.28 V bias. The forward bias direction implies a thicker collector barrier. (e) Zoom of (d). Reverse bias has a linear potential drop in the well indicating negligible electron charge in the well. Forward bias shows curvature in the well indicating electron accumulation resulting in a potential difference of about 40 meV. (f) 0.52 bias. Potential difference in the well is about 90 meV due to charge accumulation in forward bias. A higher bias must be applied in that direction to turn off the RTD.

electrostatic potential with the quantum charge in both the quantized emitter and well states is required for predictive accuracy. We find quantitative agreement between simulation and experiment for a test matrix of unstrained InGaAs/InAlAs (FIG. 12) and strained InGaAs/AlAs (FIG. 13) high current density RTDs in which barrier, well, and spacer widths are varied systematically. The material parameters are fixed and only structural changes from one device to the next are changed for all the simulations. Our charge self-consistency model is evaluated with structures which have intentional barrier asymmetry. We quantitatively model the charge accumulation/depletion inside an RTD in the forward/reverse bias direction and achieve good agreement between theory and experiment.

Our comparisons between experimental and calculated I-Vs show that the room temperature valley current of InGaAs/InAlAs and InGaAs/AlAs RTDs is determined by thermionic emission through the first excited state rather than incoherent scattering. Preliminary calculations of state-of-the-art RTDs with the InAs notched well indicate that the regime has been reached in which the room temperature valley current is determined by incoherent scattering processes rather than thermionic emission. NEMO can now be used to design devices quantitatively to address issues like the improvement of the peak-to-valley-ratio.

5.2 Scattering-limited low temperature GaAs / AlAs RTD

RTD device performance is ultimately limited by the amplitude of the off-resonant valley current due to incoherent scattering processes such as polar optical phonon (POP), acoustic phonon, interface roughness (IR) and alloy disorder scattering. The scattering mechanisms that give rise to valley currents in RTDs have been studied using a number of different approaches (for representative examples, see references [20-22]). Our approach is based on a non-equilibrium Green function formalism which includes scattering effects through self-energy terms in a truncated self-consistent Born approximation [2, 7]. This algorithm is similar to the multiple sequential scattering algorithm described by Roblin and Liou [21]. We model interface roughness as a single layer of alloy where the cations of a single species cluster into islands [2, 8]. A screened bulk Fröhlich Hamiltonian is used to model the POP interaction [2]. Since the self-energies have a strong momentum dependence, we numerically integrate over the incident transverse momenta.

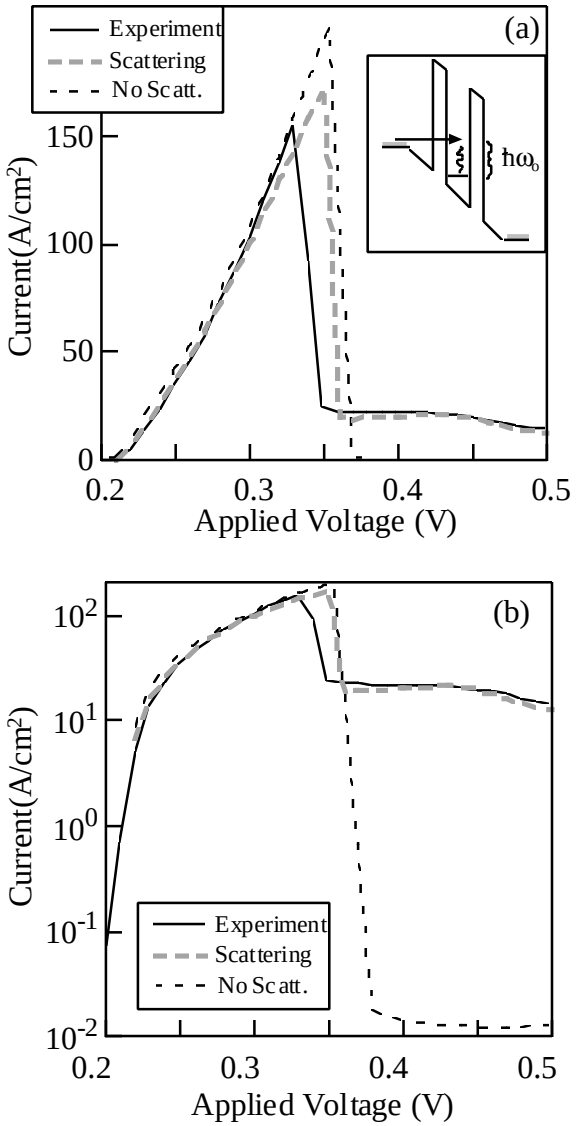

FIG. 14. Current voltage characteristic of an GaAs / AlAs resonant tunneling diode at a temperature of 4.2 K plotted on a linear (a) and logarithmic (b) scale.

The GaAs-AlAs RTD simulated here was grown by molecular-beam-epitaxy with 19.5 nm intrinsic GaAs spacer layers, 3.1 nm AlAs barriers, and a 6.2 nm GaAs well. The n^+ contacts are Si doped at 10^{18} cm^{-3}. Measurements are made at a temperature of 4.2 K to eliminate tunneling through X states in the AlAs barriers. The valley current in the region of the I-V past the current turn-off is dominated by a polar-optical-phonon assisted tunneling process illustrated in the inset of Fig. 14(a). If we neglect polar optical phonon and interface roughness scattering, the calculation of the valley current is too low and the peak-to-valley ratio is too high by 3 orders of magnitude.

5.3 MOS simulations

For the year 2010, the Semiconductor Industry Association Roadmap shows a minimum gate length of 0.07 μm. Operating MOS devices with gate lengths of 45 nm have recently been demonstrated [23]. As dimensions are reduced, quantum mechanical effects influence the device performance. The reduction in gate oxide thickness is limited by the tunneling current through the oxide. For ultra-thin oxides, the quantum charge distribution affects the gate capacitance and the threshold voltage. Tunneling through the gate depletion region is a significant contributor to the current for devices with ultra-short gate lengths of 25-30 nm.

Recent experimental work [14, 24] has been undertaken to characterize the effective mass and barrier height of ultra-thin (1.6-3.5 nm) layers of SiO_2. The experimentally measured tunnel currents versus applied voltage (I-V's) are shown in Fig. 15 for 4 different barrier thicknesses. The simulated I-V's are also plotted. The simulations accurately predict the tunnel current over a range of 10 orders of magnitude through the Al / SiO_2 / Si diodes.

In an inversion layer near a barrier such as SiO_2, the actual charge distribution can be significantly different from the semi-classically calculated charge distribution. The difference is a quantum mechanical effect. The actual charge is shifted away from the interface. This shift increases the effective barrier width and reduces the gate capacitance. The charge distributions calculated semi-classically and quantum-mechanically are shown in Fig. 16. Detailed results can be found in reference [14].

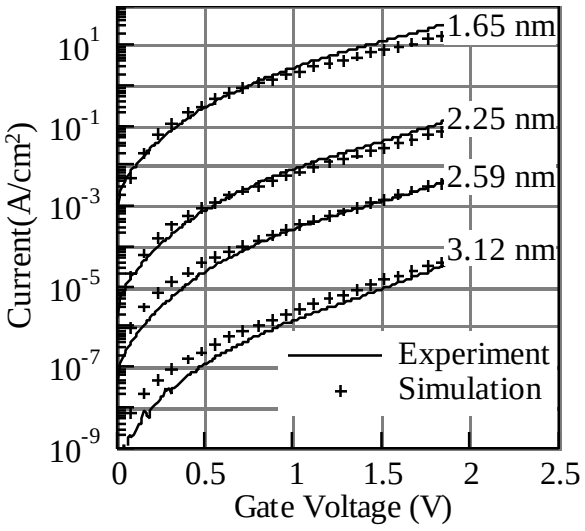

FIG. 15. Leakage current through a single SiO_2 barrier sandwiched between n-type Si and Al for several different barrier thicknesses. The experimental data are shown in a solid line and the simulation results are shown with crosses.

The distributions are significantly different in the inversion layer. The semi-classical charge distribution of NEMO has been compared for this structure to a calculation using MEDICI and identical results have been obtained.

The quantum effect on the charge distribution reduces the gate capacitance in inversion since the charge is shifted away from the barrier. Figure 17 shows the NEMO calculation of the capacitance for the structure shown in Fig. 16 for the semi-classical and quantum-mechanical charge distributions.

6. Summary

In conclusion, we have created a comprehensive, versatile, and user-friendly quantum device modeling tool. The tool has predictive capability that we have tested against a number of different devices and materials.

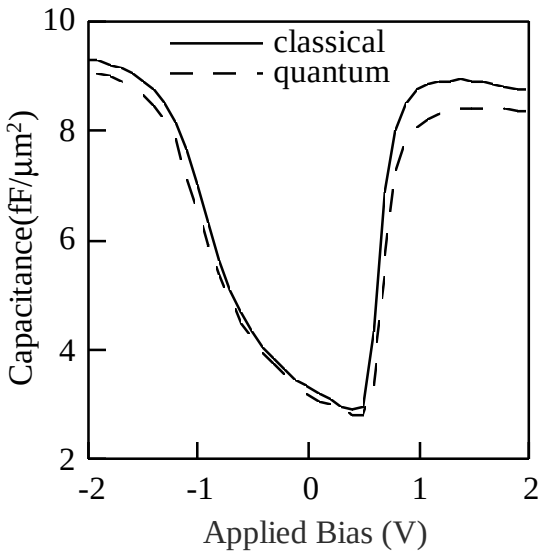

FIG. 16. Capacitance as a function of voltage calculated for a semi-classical and quantum mechanical charge distribution. In inversion the capacitance calculated quantum mechanically is reduced compared to the one calculated classically.

7. References

1. Fischetti, M.V., S.E. Laux, and E. Crabbe, *Understanding hot-electron transport in silicon devices: Is there a shortcut?* J. Appl. Phys., 1995. **78**: p. 1058.

2. Lake, R., *et al., Single and Multi-Band Modeling of Quantum Electron Transport Through Layered Semiconductor Devices.* J. Appl. Phys., 1997. **81**(12): p. 7845-7869.

3. Lake, R., *et al., Quantum Transport with Band-Structure and Schottky Contacts.* accepted in Physica Status Solidi (b), 1997.

4. Klimeck, G., *et al., Quantum device simulation with a generalized tunneling formula.* Appl. Phys. Lett., 1995. **67**(17): p. 2539--2541.

5. Klimeck, G., *et al. Nanoelelectronic Modeling (NEMO).* in *53rd Annual Device Research Conference*. 1995. Charlottesville, VA: IEEE, 53rd Annual Device Research Conference.

6. Lake, R., *et al. Experimentally verified quantum device simulations based on multiband models, Hartree self-consistency, and scattering assisted charging*. in *54th Annual Device Research Conference*. 1996. Santa Barbara, CA: IEEE, 54th Annual Device Research Conference.

7. Klimeck, G., *et al., The Effects of Electron Screening Length and Emitrter Quasi-Bound States on the Polar-Optical Phonon Scattering Resonant Tunneling Diodes.* accepted in Physica Status Solidi (b), 1997.

8. Lake, R., *et al., Interface Roughness, Polar Optical Phonons, And The Valley Current of Resonant Tunneling Diodes.* Superlattices and Microstructures, 1996. **20**(3): p. 279--85.

9. Bowen, R.C., *et al., Transmission resonances and zeros in multi-band models.* Phys. Rev. B, 1995. **52**(4): p. 2754.

10. Klimeck, G., *et al., Resolution of Resonances in a General Purpose Quantum Device Simulator.* to appear in VLSI Design, 1997.

11. Boykin, T.B., *Generalized eigenproblem method for surface and interface states: the complex bands of GaAs and AlAs.* Phys. Rev. B, 1996. **54**: p. 8107.

12. Boykin, T.B., *Tunneling calculations for systems with singular coupling matrices: results for a simple model.* Phys. Rev. B, 1996. **54**: p. 7670--3.

13. Boykin, T.B., *et al., Effective Mass reproducibility of the nearest-neighbor sp3s* models: analytic results.* accepted in Phys. Rev. B, 1997.

14. Bowen, R.C., *et al., Physical Oxode Thickness Extraction and Verification using Quantum Mechanical Simulation.* accepted in IEEE IEDM 97, 1997.

15. Gawlinski, E., T. Dzurak, and R.A. Tahir-Kheli, *Direct and exchange-correlation carrier interaction effects in a resonant tunnel diode.* J. Appl. Phys., 1992. **72**(8): p. 3562--3569.

16. Wagt, J.P.A.v.d., A.C. Seabaugh, and E. Beam, III, *RTD/HFET Low Standby Power SRAM Gain Cell.* IEDM Proceedings, 1996: p. 425-8.

17. Seabaugh, A.C., *et al.*, to be submitted to IEEE Trans. on Electr. Dev., 1997.

18. Williamson, W., III, *et al., 12 GHz Clocked*

Operation of Ultralow Power Interband Resonant Tunneling Diode Pipelined Logic Gates. IEEE J. of Solid-State Circuits, 1997. **42**(2): p. 222-30.

19. Semiconductor Industry Association, *The National Technology Roadmap for Semiconductors*. 1994.

20. Chevoir, F. and B. Vinter, *Scattering-assisted tunneling in double-barrier diodes: Scattering rates and valley current.* Phys. Rev. B, 1993. **47**: p. 7260--7273.

21. Roblin, P. and W. Liou, *Three-dimensional scattering-assisted tunneling in resonant-tunneling diodes.* Phys. Rev. B, 1993. **46**: p. 2416.

22. Lake, R. and S. Datta, *Nonequilibrium Green's-Function Method Applied to Double-Barrier Resonant-Tunneling Diodes.* Phys. Rev. B, 1992. **45**(12): p. 6670--6685.

23. Ono, M., *et al.*, *A 40 nm Gate Length n-MOSFET*. IEEE TED, 1995. **42**: p. 1822.

24. Brar, B., G.D. Wilks, and A.C. Seabaugh, *Direct Extraction of the Electron Tunneling Effective Mass in Ultrathin SiO2.* Appl. Phys. Lett., 1996. **69**(18): p. 2728--30.